Received: 7 January 2021 | Revised: 27 June 2021 | Accepted: 4 August 2021

DOI: 10.1002/mp.15166

RESEARCH ARTICLE

MEDICAL PHYSICS

A comparative study of effective atomic number calculations for dual-energy CT

Tianyu Liu[1] | **Guobin Hong**[2] | **Wenli Cai**[1]

[1] Department of Radiology, Massachusetts General Hospital and Harvard Medical School, Boston, Massachusetts, USA

[2] Department of Radiology, The Fifth Affiliated Hospital of Sun Yat-Sen University, Zhuhai, Guangdong, China

Correspondence
Wenli Cai, Mass. General Hospital / Harvard Medical School Radiology, 25 New Chardon St. 400C, Boston, MA 02114, USA.
Email: cai.wenli@mgh.harvard.edu

Funding information
National Cancer Institute, Grant/Award Number: R03CA223711

Abstract

Purpose: Several new formalisms of Effective Atomic Number (Z_{eff}) have emerged recently, deviating from the widely accepted Mayneord's definition. This comparative study aims to reexamine their theories, reveal their connections, and apply them to material differentiation on dual-energy computed tomography (DECT).

Methods: The first part of this paper is an in-depth review of several highly cited Z_{eff} formalisms. This part includes (1) refuting the claim in Taylor's study that the classic Mayneord's formalism was inaccurate, (2) showing that Mayneord's, Rutherford's, and Bourque's formalisms were equivalent, and (3) explaining the fundamental difference between Taylor's and Bourque's formalisms. The second part of this paper explains how we translated the theories into software implementation and added an open-source Z_{eff} calculation engine to our free research software 3D Quantitative Imaging (3DQI). The work includes developing an interpolation method based on radial basis function to make Taylor's formalism applicable to DECT, and devising a table lookup method to generate Z_{eff} map with high efficiency for all appropriate formalisms.

Results: Comparing Bourque's and Taylor's formalisms for six common materials over 40 $\sim$ 100 keV energy range, it was found that Bourque's Z_{eff} values had a weak energy dependence by 0.18% $\sim$ 3.10%, but for Taylor's results this variation increased by a factor of 10. Further comparison showed that at 61 keV, different formalisms fall into two categories—Bourque, Mayneord, Van Abbema (a derivative of Rutherford) for the first category, and Taylor and Manohara for the second. Formalisms within each category produced similar Z_{eff} values. For a material consisting of two elements, the two categories of formalisms tended to show a greater discrepancy if the constituent elements had larger difference in Z. The developed Z_{eff} calculation engine was successfully applied to kidney stone classification and colon electronic cleansing.

Conclusions: We renewed the understanding of several popular Z_{eff} formalisms: Contrary to the conclusion of Taylor's study, Mayneord's power-law formula is well grounded in theory; Bourque's formalism (based on the average electron microscopic cross-section) is considered numerically equivalent to Rutherford's, but with the advantage of being mathematically rigorous and physically meaningful; Taylor's formalism (based on the average atomic microscopic cross-section) is theoretically not suitable for DECT but a workaround still exists; Manohara's formalism should be used with caution due to a problem in its definition of electron cross-sections. The developed Z_{eff} engine in the 3DQI software facilitated accurate and efficient Z_{eff} estimate for various DECT applications.

KEYWORDS
dual energy CT, effective atomic number, electronic cleansing

1 | INTRODUCTION

Dual energy computed tomography (DECT) is used to classify and identify materials that otherwise have similar CT numbers in conventional single-energy CT scans.DECT acquires a pair of images at two distinct x-ray tube potentials and differentiates material on the grounds that heavier elements have more pronounced difference in photon attenuation than lighter elements at those two tube potentials. Biological materials are generally compounds and mixtures whose photon attenuation property is collectively determined by their constituent elements. As a result, the use of a single effective atomic number (EAN or Z_{eff}) to characterize the molecule of a biological material as a whole is appealing for quantitative CT analysis.

Several formalisms of Z_{eff} have been proposed and adopted over years. The classic Mayneord's[1,2] "power-law" formula (Equation 1) is commonly seen in the textbooks[3,4] and has conventionally been used in DECT research as the ground truth for materials with known elemental compositions.[5–7] In this formula, i indexes the constituent elements, m is a constant, and λ_i is the weight function. Several variations exist in the way m and λ_i are chosen, and an extensive review was conducted by Bonnin.[8]

$$Z_{\text{eff},m,\text{power}} = \left(\sum_i \lambda_i Z_i^m \right)^{\frac{1}{m}}. \tag{1}$$

Rutherford[9] extended Mayneord's formalism and devised a method to predict Z_{eff} for materials whose elemental composition is not known. This method specifically applies to DECT and derives Z_{eff} by numerically solving an equation involving the linear attenuation coefficients of materials at two different kVps. Rutherford's[9] seminal work established a theoretical foundation for many subsequent, recent studies that were aimed to improve the accuracy and practicality of Z_{eff} measurements.[5,10,11]

Bourque[12] introduced a completely new formalism with a rigorous derivation. Based on Yang's[13] approach, Bourque's formalism allows for a clearer interpretation of Z_{eff} by considering the average electron microscopic cross-sections. Bourque also formulated a practical strategy to estimate Z_{eff} for DECT based on stoichiometric calibration.

Another new formalism by Taylor[14] emerged recently. This study appeared surprisingly disruptive in that it disputed the validity of the long-held Mayneord's power-law formula, dismissing it as "inaccurate," "dubious," "dated," and "overly simplistic." Taylor reported substantial discrepancy between the two formalisms and claimed theirs to be a valid and accurate alternative. In a similar vein, Manohara[15] proposed a new formalism differing widely from the classic approach, where the cross-section parameterization step as in Mayneord's[1,2] and Rutherford's[9] formalisms was completely avoided.

The first purpose of this study is to compare these highly cited definitions of Z_{eff} mentioned above and provide our insight into their relations. Specifically, we make the following important points: (1) Unlike what was claimed in Taylor's study,[14] Mayneord's formalism is actually solid in its theoretical footing. (2) Despite taking a different path of derivation, Bourque's formalism can be considered equivalent to Mayneord's and Rutherford's. Although various Z_{eff} formalisms exist, according to their numerical values they boil down to two main categories: Bourque's and Taylor's. (3) Although Taylor's formalism generally leads to different Z_{eff} values, under certain conditions it approaches Bourque's. (4) A problem existing in the highly cited Manohara's formalism is identified. To the best of our knowledge, comparative study of such kind is scarce in the literature.

As the second part of this study, we discuss how Bourque's and Taylor's formalisms were implemented in a Z_{eff} calculation engine we developed for DECT applications. This engine is part of our free research software 3D Quantitative Imaging (3DQI).

2 | MATERIALS AND METHODS

2.1 | A comparative review

In this section, we review and comment on several highly cited formalisms of Z_{eff}. In addition to examining the theoretical basis of each formalism, we seek to explain their connections. For the sake of clarity, equations and notations may be modified as needed and appear different from their original forms.

2.1.1 | Classic formalism

The most influential formalism by Mayneord[1] and Spiers[2] started with Equation (2), where the linear attenuation coefficient μ_m is expanded as the weighted sum of total microscopic cross-sections of the constituent elements σ_i (ρ is the material density, N_A is the Avogadro constant, A is the molar mass, and n_i is the number of atoms of the ith element in the molecule). Mayneord considered the contributions from photoelectric effect and incoherent scattering, and parameterized their microscopic cross-sections using Equations (3) and (4), respectively, where k is a constant, E is the photon energy, and $\epsilon(E)$ is the Klein–Nishina cross-section per electron.

$$\begin{aligned} \mu_m &= \frac{\rho N_A}{A} \sum_i n_i \sigma_i, \\ &\approx \frac{\rho N_A}{A} \sum_i n_i (\sigma_{PE,i} + \sigma_{INC,i}), \end{aligned} \tag{2}$$

$$\sigma_{PE} \approx kE^{-3}Z^{m+1} \quad \text{(photoelectric effect)}, \tag{3}$$

$$\sigma_{INC} \approx Z\epsilon(E) \quad \text{(incoherent scattering)}. \tag{4}$$

This enables Equation (2) to be rearranged into Equation (5). Note how the term $\sum_i n_i Z_i$ is ingeniously separated from the sum.

$$\begin{aligned}\mu_m &\approx \frac{\rho N_A}{A}\sum_i n_i Z_i\left(\epsilon(E) + kE^{-3}Z_i^m\right)\\ &= \frac{\rho N_A}{A}\left(\sum_i n_i Z_i \epsilon(E) + \sum_q n_q Z_q \sum_i \frac{n_i Z_i}{\sum_q n_q Z_q} kE^{-3}Z_i^m\right)\\ &= \frac{\rho N_A}{A}\left(\sum_i n_i Z_i\right)\left(\epsilon(E) + kE^{-3}\sum_i \lambda_i Z_i^m\right)\\ &\equiv \frac{\rho N_A}{A}\left(\sum_i n_i Z_i\right)\left(\epsilon(E) + kE^{-3}Z_{\text{eff},m,\text{power}}^m\right),\end{aligned} \tag{5}$$

where λ_i is the fraction of the ith element by the number of electrons:

$$\lambda_i = \frac{n_i Z_i}{\sum_i n_i Z_i}. \tag{6}$$

From Equation (5), Mayneord defined the "power-law" form of EAN in Equation (1). The value of m is chosen differently in the literature, such as 2.94,[1,2] 3.1,[16] 3.5,[3] 3.3.[17] $Z_{\text{eff},m,\text{power}}$ is frequently used as the theoretical baseline in studies pertaining to DECT.[5,17,18]

The approximations residing in Mayneord's formalism are primarily introduced by the use of Equation (2), which ignores contribution from other photoatomic processes, and Equations (3) and (4), which fit the actual cross-section to a limited degree.

It should be emphasized that despite these approximations and the apparently simple form, the power-law formula itself is theoretically sound for CT energy range, and that the inherent energy independence of $Z_{\text{eff},m,\text{power}}$ is a desirable property preventing CT-based material differentiation from sustaining spectrum-related uncertainty. Previous study by Taylor[14] overlooked these facts and their claim that the power-law formula significantly overestimates Z_{eff} is incorrect.

2.1.2 | Rutherford's formalism

Rutherford[9]'s formalism followed Mayneord's approach to cross-section parameterization, and improved the accuracy by including a correction term $\delta(Z, E)$, taking account of the coherent scattering and electron binding effect, shown in Equation (7),

$$\begin{aligned}\sigma(Z,E) &= \sigma_{PE}(Z,E) + \sigma_{INC}(E) + \delta(Z,E)\\ &\approx \hat{\sigma}_r(Z,E) \equiv aE^bZ^c + \epsilon(E)Z + dE^fZ^g \quad Z \in \mathbb{N},\end{aligned} \tag{7}$$

where $\hat{\sigma}_r(Z, E)$ denotes the parametric equation, and $a \sim g$ are constants.

Rutherford re-examined the linear attenuation coefficients of mixtures μ_m, and extended the definition of Z from elements ($Z \in \mathbb{N}$) to mixtures ($Z \in \mathbb{R}$) by introducing two new quantities, the effective atomic number $Z_{\text{eff},m,r}$ and the effective number of atoms per unit volume $N_{\text{eff},m,r}$ that satisfy Equation (8), where E_1 and E_2 are effective energies of two different tube potentials.

$$\begin{aligned}\mu_m &= N\sum_i n_i\sigma_i\\ &= \sum_i \hat{\sigma}_r(Z_i,E)(Nn_i) \quad Z_i \in \mathbb{N}\\ &\equiv \hat{\sigma}_r(Z_{\text{eff},m,r},E_k)N_{\text{eff},m,r} \quad Z_{\text{eff},m,r} \in \mathbb{R}, k = 1,2.\end{aligned} \tag{8}$$

Rutherford then obtained Equation (9) where $N_{\text{eff},m,r}$ is cancelled out and $Z_{\text{eff},m,r}$ becomes numerically solvable.

$$\frac{\mu_{E_1}}{\mu_{E_2}} = \frac{\hat{\sigma}_r(Z_{\text{eff},m,r},E_1)}{\hat{\sigma}_r(Z_{\text{eff},m,r},E_2)}. \tag{9}$$

There are three issues in Rutherford's formalism.

1. The physical meaning of $Z_{\text{eff},m,r}$ and $N_{\text{eff},m,r}$ is obscure, and whether the cross-section parameterization for elements still applies to mixtures is not well explained.
2. Equation (9) assumes that $Z_{\text{eff},m,r}$ remains unchanged at E_1 and E_2, but omits to discuss whether such energy independence holds for a continuous range of energy. Invariance of $Z_{\text{eff},m,r}$ is important in that it ensures the root of Equation (9) remains stable when the effective energy values fluctuate.
3. The assumption that Equation (9) has a unique, positive real root is not sufficiently validated.

Despite these imperfections, Rutherford has heavily influenced later studies, such as Torikoshi,[10] Bazalova,[11] Van Abbema.[19] Torikoshi[10] improved the validity of Equation (9) to some extent by verifying that Z_{eff} of water only slightly varied with energy (with less than 1% variation) for $E1 \in [30, 60]$ keV, $E2 \in [60, 150]$ keV.

2.1.3 | Bourque's formalism

Bourque[12] is among the very few to provide a rigorous definition of Z_{eff} for mixtures. The centerpiece of their formalism is parameterization of *average electron microscopic cross-sections* σ_e, which was originally adopted by Yang.[13] For elements, at a certain photon energy, σ_e is defined in Equation (10), and approximated by the parametric equation $\hat{\sigma}_{e,bq}(Z)$, which is an M degree polynomial in a single variable Z. It is worth adding that such parametrization is validated by Weierstrass approximation theorem, which states that continuous, real-valued functions can be uniformly approximated by polynomials on a close and bounded interval.[20]

$$\begin{aligned}\sigma_e &= \frac{\sigma}{Z} \quad Z \in \mathbb{N} \\ &\approx \hat{\sigma}_{e,bq}(Z) \equiv \sum_{m=0}^{M} a_m Z^m, \quad Z \in \mathbb{N}.\end{aligned} \tag{10}$$

For mixtures, the average electron microscopic cross-section is defined in Equation (11). With a few more steps, $\sigma_{e,m}$ can be expressed in terms of $\sigma_{e,i}$ of the constituent elements.

$$\sigma_{e,m} = \frac{\sigma_m}{\sum_i n_i Z_i} = \frac{\sum_i n_i \sigma_i}{\sum_i n_i Z_i} = \sum_i \lambda_i \frac{\sigma_i}{Z_i} = \sum_i \lambda_i \sigma_{e,i}, \tag{11}$$

where σ_m is the total microscopic cross-section of the mixture and λ_i is defined in Equation (6).

Bourque extended the definition of Z from elements ($Z \in \mathbb{N}$) to mixtures ($Z \in \mathbb{R}$) by Equation (12), on the premise that $\hat{\sigma}_{e,bq}(Z)$ is a bijective function at the energy considered. Bourque showed that the bijective relation holds true for $Z \in [1, 52]$ within the common energy range for DECT.

$$Z_{\text{eff},m,bq} = \hat{\sigma}_{e,bq}^{-1}(\sigma_{e,m}) \quad Z_{\text{eff},m,bq} \in \mathbb{R}. \tag{12}$$

One of the main advantages of Bourque is that the effective quantities $\hat{\sigma}_r(Z_{\text{eff},m,bq})$ and $N_{\text{eff},m,r}$ in Equation (8) that previously had vague physical meanings in Rutherford can now be concretely defined as $\hat{\sigma}_r(Z_{\text{eff},m,bq}) = Z_{\text{eff},m,bq}\hat{\sigma}_{e,bq}(Z_{\text{eff},m,bq})$ and $N_{\text{eff},m,r} = \frac{N}{Z_{\text{eff},m,bq}} \sum_i n_i Z_i$. This clear definition resolves issue (1) in Rutherford.

For common biological materials, $Z_{\text{eff},m,bq}$ is numerically insensitive to energy in general, and the weak energy dependence for some energy ranges and some materials is treated as a source of nonstatistical uncertainty of Z_{eff}.[12] Specifically, the variation is found to be on the order of 0.2% of Z_{eff} for the x-ray spetra of two DECT scanners: SOMATOM Definition Flash (Siemens) and Gemini GXL (Philips).[12] This result avoids issue (2) in Rutherford.

Besides, Bourque investigated the energy-dependence of dual energy ratio (DER) Γ (Equation (13) where w refers to water, $E1 < E2$) and observed the bijective relation between Z and Γ for $Z \in [1, 38]$. This illustrates the existence of a unique, positive real root of Z_{eff} in Equation (9) and avoids issue (3) in Rutherford.

$$\Gamma \equiv \frac{\frac{\mu_{E1}}{\mu_{E1,w}}}{\frac{\mu_{E2}}{\mu_{E2,w}}}. \tag{13}$$

Notably, Bourque proposed a stoichiometric calibration approach for Z_{eff} calculation of unknown material that does not take the form of Equation (9). In this approach, Z_{eff} is simply expressed in terms of Γ in a polynomial form (Equation 14). The coefficients c_k were determined by curve fitting, given the calculated values of Z_{eff} of a multi-material calibration phantom and the measured values of Γ. The chief advantage of this approach is that c_k takes into account the x-ray spectra, eliminating the need for spectrum measurement or monochromatic energy approximation. Bourque's formalism completes the theoretical basis for Rutherford's. The former is effectively a sufficient condition for the latter.

$$Z_{\text{eff},m,bq} = \sum_{k=1}^{K} c_k \Gamma^{k-1}. \tag{14}$$

2.1.4 | Taylor's formalism

Following Rao's[21] approach, Taylor[14] redefined Z_{eff} using the *average atomic microscopic cross-section* σ_a. For elements, σ_a is approximated by the parametric equation $\hat{\sigma}_{a,tl}(Z)$ defined in Equation (15).

$$\sigma_a \approx \hat{\sigma}_{a,tl}(Z) \equiv \sum_j Q_j N_{j,d}(Z) \quad Z \in \mathbb{N}, \tag{15}$$

where $N_{j,d}(Z)$ is the B-spline basis function of d degree and Q_j is the B-spline control points.

For mixtures, Taylor provided the definition of average atomic microscopic cross-section in Equation (16).

$$\sigma_{a,m} = \frac{\left(\frac{\mu}{\rho}\right)_m}{N_A \sum_i \frac{w_i}{A_i}}, \tag{16}$$

where $(\frac{\mu}{\rho})_m$ is the mass attenuation coefficient of the mixture, and w_i is the fraction of the ith element by

weight. The physical meaning of $\sigma_{a,m}$ is not immediately obvious from Equation (16), but can be easily revealed: Given that $w_i = \frac{n_i A_i}{A}$ and that $(\frac{\mu}{\rho})_m = \frac{N_A}{A}\sum_i n_i\sigma_i$, it follows that

$$\sigma_{a,m} = \frac{\sum_i n_i\sigma_i}{\sum_i n_i} = \sum_i f_i\sigma_i, \tag{17}$$

where

$$f_i = \frac{n_i}{\sum n_i} \tag{18}$$

is the fraction of the ith element by the number of atoms. Equation (17) indicates that $\sigma_{a,m}$ is in fact the molecular microscopic cross-section averaged over all constituent atoms.

Given a mixture, Taylor first calculates $\sigma_{a,m}$ at the energy of interest, then derives Z_{eff} from the B-spline parametric equation $\hat{\sigma}_{a,tl}(Z)$. A formal definition of Z_{eff} can be made by Equation (19) in a similar way to Bourque, on the same premise that $\hat{\sigma}_{a,tl}(Z)$ is a bijective function within certain ranges of energy and Z values.

$$Z_{\text{eff},m,tl} = \hat{\sigma}^{-1}_{a,tl}(\sigma_{a,m}) \quad Z_{\text{eff},m,tl} \in \mathbb{R}. \tag{19}$$

2.1.5 | Comparison between Bourque's and Taylor's formalisms

The fundamental difference between Bourque's and Taylor's formalisms of Z_{eff} lies in parameterizing different types of microscopic cross-sections. There are two consequences.

The first is that, the microscopic cross-sections of the constituent elements are weighted differently in calculating that of a mixture (λ_i for $\sigma_{e,m}$ in Bourque, whereas f_i for $\sigma_{a,m}$ in Taylor), therefore leading to different Z_{eff} values of the mixture.

Suppose the chemical formula of a mixture is arranged such that the K constituent elements are sorted in ascending order of Z, that is, $Z_1 < Z_2 < ... < Z_K$. Consider the difference between the two types of weight:

$$\begin{aligned}\delta_i &= f_i - \lambda_i \\ &= \frac{n_i}{\sum n_i} - \frac{n_i Z_i}{\sum_i n_i Z_i} \\ &= \frac{n_i(n_1(Z_1 - Z_i) + n_2(Z_2 - Z_i) + \cdots + n_K(Z_K - Z_i))}{\sum_i n_i Z_i \sum_i n_i}.\end{aligned} \tag{20}$$

It is easily seen that

$$\delta_1 = \frac{n_1(0 + n_2(Z_2 - Z_1) + \cdots + n_K(Z_K - Z_1))}{\sum_i n_i Z_i \sum_i n_i} > 0$$

$$\delta_K = \frac{n_K(n_1(Z_1 - Z_K) + n_2(Z_2 - Z_K) + \cdots + 0)}{\sum_i n_i Z_i \sum_i n_i} < 0$$

$$\delta_1 > \delta_2 > ... > \delta_K. \tag{21}$$

It follows that (1) elements with a smaller atomic number have greater weight in Taylor than in Bourque, hence $Z_{\text{eff},m,tl} < Z_{\text{eff},m,bq}$, and that (2) the greater the difference between the atomic numbers of the constituent elements, the greater the range δ_i spans, and the greater the difference between the resulting $Z_{\text{eff},m,tl}$ and $Z_{\text{eff},m,bq}$.

For example, common biological materials typically contain hydrogens ($Z = 1$), thereby their $Z_{\text{eff},m,tl}$ values being significantly lower than $Z_{\text{eff},m,bq}$. In contrast, the air does not have hydrogens, and the difference between $Z_{\text{eff},m,tl}$ and $Z_{\text{eff},m,bq}$ is much smaller. This will be shown in 3.2.

The second consequence is that, $Z_{\text{eff},m,tl}$ and $Z_{\text{eff},m,bq}$ have different numerical sensitivity to energy. Yang[13] noted that Z_{eff} only slowly varies with energy if derived from $\sigma_{e,m}$, but varies strongly with energy if $\sigma_{a,m}$ is used instead. This is more clearly illustrated in Figure 1: For a material composed of two elements, the $\sigma_{e,m}$ values calculated at low and high energies correspond to nearly the same $Z_{\text{eff},m,bq}$ values (18.43 and 18.44), whereas $\sigma_{a,m}$ values to markedly different $Z_{\text{eff},m,tl}$ values (10.56 and 8.41).

2.1.6 | Manohara's formalism

Another highly cited formalism was proposed by Manohara,[15] which results in a simple analytical expression shown in Equation (22).

$$Z_{\text{eff},m,ma} = \frac{\sigma_{a,m}}{\widetilde{\sigma}_{e,m}}, \tag{22}$$

where $\widetilde{\sigma}_{e,m}$ is defined as the effective electron microscopic cross-section given by Equation (23).

$$\begin{aligned}\widetilde{\sigma}_{e,m} &= \frac{\sum_i \frac{n_i\sigma_i}{Z_i}}{\sum_i n_i} \\ &= \sum_i f_i\sigma_{e,i}.\end{aligned} \tag{23}$$

This formalism should be used with caution, as Equation (23) turns out to be questionable on close exami-

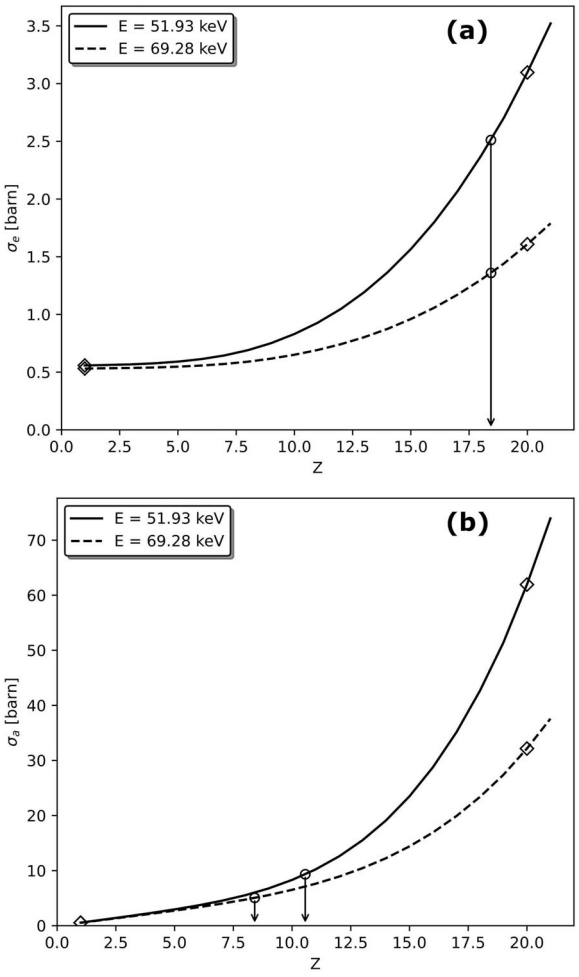

FIGURE 1 $Z_{\text{eff},m,bq}$ and $Z_{\text{eff},m,tl}$ show different levels of energy dependence for a fictitious compound CaH_6. The solid and dotted lines are the EAN—cross-section curves obtained at the mean energy values 51.93 keV and 69.28 keV (for the 80–140 kVp spectra), respectively. The x-coordinates of the squares are Z of the constituent elements, whereas those of the circles are Z_{eff} of the compound. (a) For Bourque's formalism based on σ_e, the calculated $Z_{\text{eff},m,bq}$s at different energies are approximately identical. (b) For Taylor's formalism based on σ_a, $Z_{\text{eff},m,tl}$s at different energies are markedly different

nation. The average (or effective) electron microscopic cross-section is a derived quantity, defined naturally as the molecular microscopic cross-section per electron, and formally by Equation (11) where λ_i is the weight function. However, Manohara's formalism chooses f_i as the weight function of $\sigma_{e,i}$, giving $\widetilde{\sigma}_{e,m}$ no clear physical meaning. Incidentally, if the correct definition of $\sigma_{e,m}$ is used instead, Equation (22) reduces to a trivial form (Equation 24) where the cross-section terms are simply canceled out.

$$Z_{\text{eff},m,\text{trivial}} = \frac{\sigma_{a,m}}{\sigma_{e,m}} = \frac{\sum_i n_i Z_i}{\sum_i n_i}. \tag{24}$$

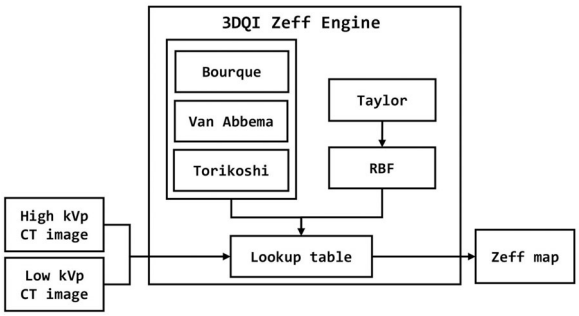

FIGURE 2 Workflow of the Z_{eff} engine developed in this study. Formalisms with weak energy dependence in Z_{eff}—such as Bourque, Van Abbema, and Torikoshi—were directly implemented to generate the Z_{eff} lookup table, while those with strong energy dependence in Z_{eff}—such as Taylor—were implemented by applying radial basis function (RBF) on $Z_{\text{eff,ave}} = \frac{Z_{\text{eff},m,tl}(E_{\text{high}})+Z_{\text{eff},m,tl}(E_{\text{low}})}{2}$ values of a select list of materials

2.2 | Development of a Z_{eff} calculation engine

As the second task of this study, we developed a Z_{eff} calculation engine for DECT application. This section dives into the software implementation detail.

2.2.1 | Software development

The engine was developed as a C++ library and integrated into our free research software 3DQI. The library offered both C++ and Python Application Programming Interfaces (APIs), the latter being open-source (https://github.com/3dqi/duo). As Van Abbema's formalism involves numerically solving equations and is computationally intensive, this part was GPU-accelerated using Heterogeneous-Computing Interface for Portability[22] to support both Nvidia and AMD GPUs.

The workflow of the engine is illustrated in Figure 2. The high and low kVp CT images are denoised separately and then passed to the engine, which generates an output of Z_{eff} map according to the user-specified formalism and the kVp setups. Currently four formalisms have been implemented, including those by Bourque, Van Abbema, Torikoshi, and Taylor, and four kVp setups supported, including 80–140 kVp with/without tin filtration, 100–140 kVp with/without tin filtration.

We applied a table lookup approach to further increase the software efficiency. Specifically, considering that the CT numbers are discrete and that there exist only finite pairs of CT numbers for the high and low kVp images, we pre-calculated—for each Z_{eff} formalism and each scan protocol—a Z_{eff} lookup table of size 4096×4096. The table iterates all combinations of $HU_{E_{\text{high}}}$ and $HU_{E_{\text{low}}}$ and the range of each HU value is $[-1000, 3095]$. At runtime, the engine no longer needs to perform additional calculation but instead

simply queries the Z_{eff} values from the table according to the given pairs of CT numbers. This approach has effectively eliminated the computational burden at the cost of a mere 128 MB ($4096 \times 4096 \times 8$ bytes) increase in memory usage. The four formalisms implemented in our engine only differ in the way their lookup tables are pre-calculated, described in the following sections.

2.2.2 | Z_{eff} lookup tables for Bourque's formalism

Bourque's formalism is deemed an ideal option due to its rigorous derivation and energy-insensitive property. Its lookup table was generated by:

1. According to the manufacturer-provided mean energy values of the high and low kVp spectra E_{high} and E_{low}, calculate the DER values (Γ, defined in Equation 13) for elements $Z = 1, 2, \ldots, Z_{\max}$.
2. Construct a function $Z_{\text{eff}}(\Gamma)$ by curve-fitting to the calculated (Γ, Z) data. $Z_{\text{eff}}(\Gamma)$ is a monotonically increasing function.
3. For the given $(HU_{E_{\text{high}}}, HU_{E_{\text{low}}})$ pair, calculate Γ. Clamp Γ if it is less than $\Gamma_{Z=1}$ or greater than $\Gamma_{Z=Z_{\max}}$.
4. Find Z_{eff} from $Z_{\text{eff}}(\Gamma)$.
5. Repeat step 3 and 4 for all combinations of $HU_{E_{\text{high}}}$ and $HU_{E_{\text{low}}}$.

It should be mentioned that in step 2, we used cubic B-spline for curve fitting in place of Bourque's polynomial approximation in Equation (10). This was found to be able to improve the overall goodness of fit for $\sigma_e(Z_{\text{eff}})$ and $\sigma_e(E)$ profiles.

2.2.3 | Z_{eff} lookup tables for Van Abbema's formalism

Rutherford's formalism and its derivatives (e.g., Van Abbema's, Torikoshi's) are equivalent to Bourque's. Instead of constructing the monotonic function $Z_{\text{eff}}(\Gamma)$, they derived Z_{eff} by solving Equation (9). The main difference between Rutherford's derivatives themselves lies in the choice of parametric form for $\hat{\sigma}_r(Z, E)$. For Van Abbema's formalism, for instance, the following steps were taken to generate its lookup tables:

1. Calculate $E_{\text{ave}} = (E_{\text{high}} + E_{\text{low}})/2$, where E_{high} and E_{low} are manufacturer-provided mean energy values of the high and low kVp spectra.
2. Determine the parametric equation $\hat{\sigma}_r(Z, E) = aE^bZ^c + dE^fZ^g + he^{-jE}Z^k$. The parameters b, f, j were derived by fitting the cross-section of oxygen for $50 \sim 100$ keV; c, g, k by fitting the cross-section at E_{ave} for $Z = 6, 7, \ldots, 20$; a, d, h by using the cross-section of oxygen at E_{ave}.[19]
3. For the given $(HU_{E_{high}}, HU_{E_{low}})$ pair, solve Equation 9 for Z_{eff} using Newton-Raphson method. Root may not exist for some physically impossible combinations, in which case set Z_{eff} to 0.
4. Repeat step 3 for all combinations of $HU_{E_{high}}$ and $HU_{E_{low}}$.

2.2.4 | Z_{eff} lookup tables for Taylor's formalism

In general, for a formalism of Z_{eff} to be suitable to DECT application, the Z_{eff} value should stay constant in the CT energy range. Strictly speaking, Taylor's[14] formalism does not qualify because of the high energy dependence. However, some materials may have constituent elements that span only a small range of Z, and according to the analysis in 2.1.5, the discrepancy between $Z_{\text{eff},m,tl}(E_{\text{high}})$ and $Z_{\text{eff},m,tl}(E_{\text{low}})$ may appear smaller ($\lesssim 10\%$). Under this circumstance, a mapping between $(HU_{E_{\text{high}}}, HU_{E_{\text{low}}})$ and $Z_{\text{eff},m,tl}$ can still be found.

The basic idea is to place a list of base materials on the $HU_{E_{\text{high}}}$ / $HU_{E_{\text{low}}}$ grid and calculate their $Z_{\text{eff,ave}} = \frac{Z_{\text{eff},m,tl}(E_{\text{high}}) + Z_{\text{eff},m,tl}(E_{\text{low}})}{2}$ values to represent $Z_{\text{eff},m,tl}$ for DECT. An unknown material whose $(HU_{E_{\text{high}}}, HU_{E_{\text{low}}})$ is located in the vicinity of those base materials is considered a mixture of them and its $Z_{\text{eff,ave}}$ is obtained by radial basis function (RBF)-based interpolation. The $Z_{\text{eff,ave}}$ lookup table is obtained by the following steps:

1. Select a list of base materials, including (1) 16 reference materials from NIST ASTAR and PSTAR programs,[23] including adipose tissue (ICRU-44), breast tissue (ICRU-44), liquid water, gray/white matter in brain (ICRU-44), testis (ICRU-44), ovary (ICRU-44), skeletal muscle (ICRU-44), soft tissue (ICRU-44), soft tissue (ICRU Four-Component), lung tissue (ICRU-44), eye lens (ICRU-44), whole blood (ICRU-44), dry air (near sea level), cortical bone (ICRU-44), A-150 tissue-equivalent plastic, B-100 bone-equivalent plastic, and (2) application-specific custom materials. For Z_{eff}-based colon electronic cleansing (EC), for instance, this includes 20 mg/ml iodine solution, iodine solution mixed with 10%, 20%, …, 90% air by volume.
2. Calculate $HU_{E_{\text{high}}}$ and $HU_{E_{\text{low}}}$ for each material on the list.
3. Calculate $Z_{\text{eff,ave}}$ for each material on the list.
4. Construct the following function by curve-fitting to the calculated $(HU_{E_{\text{high}}}, HU_{E_{\text{low}}}, Z_{\text{eff,ave}})$ data.

$$Z_{\text{eff,ave}}(HU_{E_{\text{high}}}, HU_{E_{\text{low}}}) = \sum_{i=1}^{N} w_i \phi\left(\sqrt{(HU_{E_{\text{high}}} - HU_{E_{\text{high},i}})^2 + (HU_{E_{\text{low}}} - HU_{E_{\text{low},i}})^2}\right),$$

where i indexes the predetermined material on the list, $\phi(r) = r^2\ln(r)$ is the thin plate spline, a type of radial basis function.

5. Calculate $Z_{\text{eff,ave}}$ for all combinations of $HU_{E_{\text{high}}}$ and $HU_{E_{\text{low}}}$.

It should be stressed that this makeshift approach is valid only for materials whose $Z_{\text{eff},m,tl}$ has lesser degree of energy dependence. If the application-specific base materials in step 1 do not satisfy this condition, a small change in the choice of effective energy will cause substantial shift in $Z_{\text{eff,ave}}$ values, and the predicted $Z_{\text{eff,ave}}$ of unknown materials will suffer from high uncertainty.

2.2.5 | Photoatomic cross-section data

In this study, the linear attenuation coefficients were calculated based on the latest photoatomic microscopic cross-section data from the ENDF/B-VIII.0 nuclear data library.[24] This library includes the recent experimental data by international collaboration, and benefits from the improvements in both theory and simulation.[24]

There are two considerations when using this library. (1) In ENDF/B-VIII.0, microscopic cross-section data of different photoatomic processes use different energy grid. Although the total cross-section data for each element are tabulated as well, the library explicitly advises against interpolating between them to avoid reduced accuracy. Instead, wherever the total cross-section σ, the average electron microscopic cross-section σ_e, the total mass attenuation coefficient $(\frac{\mu}{\rho})$, or the total linear attenuation coefficient μ at a certain energy are needed, they should be calculated on the fly, taking into account all the photoatomic processes. For example, σ of oxygen at 60 keV photon energy should be calculated by summing six separately interpolated microscopic cross-section data: incoherent scattering (Compton scattering), coherent scattering (Rayleigh scattering), and photoelectric effect with 1s1/2, 2s1/2, 2p1/2, and 2p3/2 atomic electrons. (2) ENDF/B-VIII.0 recommends using linear–linear interpolation for the photoatomic microscopic cross-section data.

3 | RESULTS

3.1 | Calculation of Z_{eff} lookup table

The developed Z_{eff} engine calculated Z_{eff} lookup tables for common kVp combinations, including 80–140 kVp with/without tin filtration and 100–140 kVp with tin filtration. In Bourque's study, the bijective relation between Γ and Z exists for $Z \in [1, 38]$ in all kVp combinations, while in our study that relies on ENDF/B-VIII.0 library, such relation is observed for $Z \in [1, 36]$.

Figure 3 shows the Z_{eff} tables for 80–140 kVp without tin filtration following Bourque, Van Abbema, and Taylor's formalisms. Between two dotted lines is the region $Z_{\text{eff}} \in [1, 36]$ where common materials scanned by DECT are expected to fall within. For Bourque's method in Figure 3(a), the physically invalid combinations of $(HU_{E_{\text{high}}}, HU_{E_{\text{low}}})$ whose DER values are below $\Gamma_{Z=1} = 0.915$ were assigned a Z_{eff} value of 1 (dark purple region). Those combinations where $Z_{\text{eff}} > 36$ and the bijective relation between Z and Γ breaks were assigned a Z_{eff} value of 36 (yellow region).

As is seen in Figure 3(b), Van Abbema yielded the same results with Bourque for $Z_{\text{eff}} \in [4, 20]$. Outside this range, the root of Equation (9) was not found and Z_{eff} was set to 1. This indicates that in addition to the slow computation, another disadvantage of Van Abbema's formalism is the narrower Z_{eff} range in comparison with Bourque.

The $Z_{\text{eff,ave}}$ table derived from Taylor's formalism is shown in Figure 3(c). Compared to Bourque, the base materials selected for EC application (red circles represent reference NIST materials, and yellow crosses custom materials) generally had much smaller $Z_{\text{eff,ave}}$ values except for the air located at the bottom left corner.

3.2 | Comparison of Z_{eff} values by different formalisms

3.2.1 | Numerical experiments using reference materials

This section compares Z_{eff} values calculated by various formalisms implemented in our developed Z_{eff} engine. First, we focused on Bourque and Taylor, the most highly cited ones representative of two parameterization strategies (σ_e vs. σ_a). Six common materials over the energy range [40, 100] keV were considered. It can be seen from Figure 4 that Bourque has the advantage of superior energy independence. For the air, soft tissue, cortical bone, lung, adipose tissue, and iodine solution, the variation in Z_{eff}, defined as $\frac{Z_{\text{eff,max}} - Z_{\text{eff,min}}}{Z_{\text{eff,max}} + Z_{\text{eff,min}}}$, was found to be only 0.18%, 0.74%, 0.29%, 0.61%, 1.17%, and 3.10% by Bourque. These values, however, increased to 1.19%, 10.63%, 22.06%, 11.59%, 7.23%, and 31.76% by Taylor.

We extended the comparison to other prominent formalisms such as Mayneord, Van Abbema, and Manohara, and calculated Z_{eff} values at 60.61 keV, which is the arithmetic mean of the mean energy values of 80–140 kVp spectra without tin filtration. Figure 5(a) shows that the five formalisms considered can be put into two categories, (1) Bourque, Mayneord, and Van Abbema and (2) Taylor and Manohara. For those six common materials, formalisms in the same category give similar numerical results. As is analyzed in

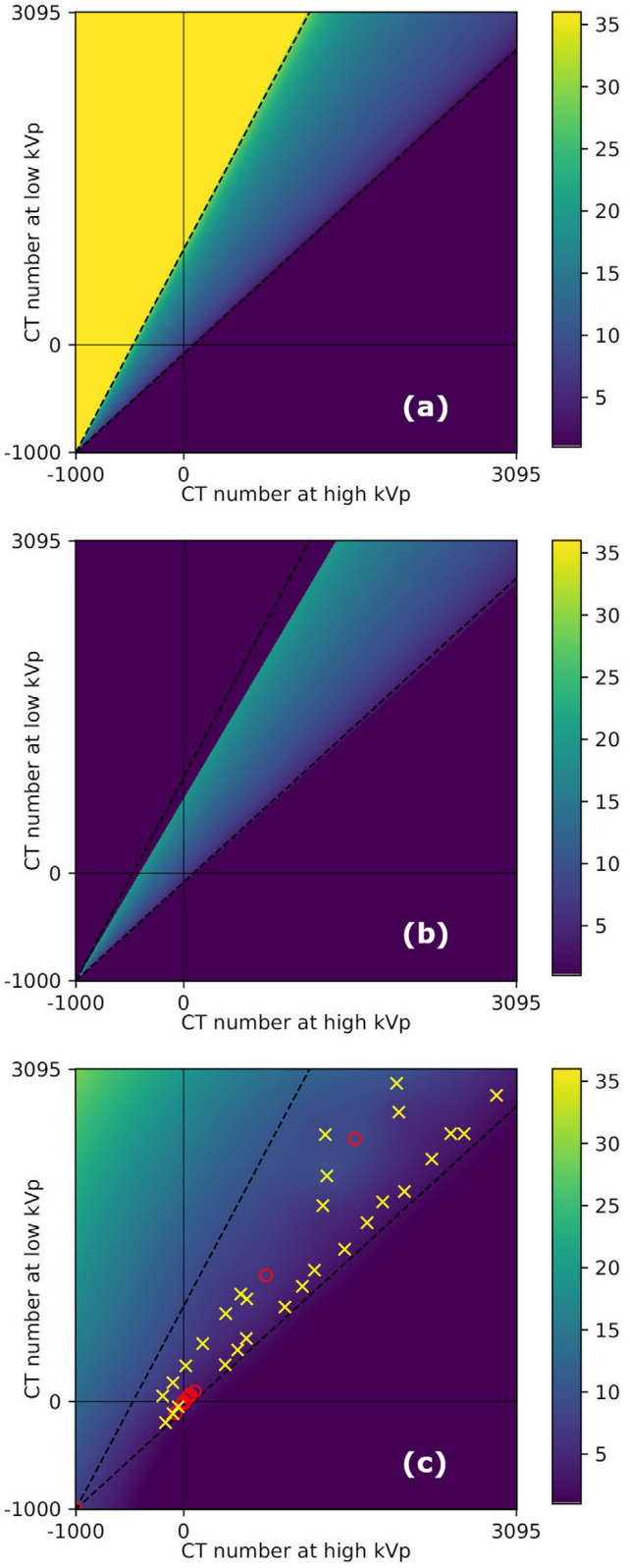

FIGURE 3 The calculated Z_{eff} lookup tables. (a) By Bourque's formalism. (b) By Van Abbema's formalism. (c) By Taylor's formalism, using RBF-based interpolation. The red circles are 16 reference materials from NIST ASTAR and PSTAR programs, while the yellow crosses are custom base materials for EC application

2.1.3, Taylor's formalism biases Z_{eff} toward lighter elements particularly when the constituent atoms of a material span a wider range of Z. The biological materials and iodine solution therefore were found to have much smaller Z_{eff} values by Taylor's formalism than those by Bourque's due to the presence of hydrogens ($Z = 1$). In comparison, minor discrepancy between Taylor and Bourque was observed for air, although the former was still consistently smaller than the latter.

Note that larger discrepancy between Taylor's and Manohara's formalisms outside the range of 0.1∼5 MeV was previously reported,[25] and that their coincidental numerical agreement at the energy considered in this study does not serve to justify Manohara's formalism for practical use.

For further analysis, we considered a fictitious material $Ca\Phi_2$, where the atomic number of element Φ is set to $Z = 1, 2, \ldots 19$. Figure 5(b) shows that for such material Z_{eff} values can still be put into the same two categories. At $Z_\Phi = 1$, Taylor's result is smaller than Bourque's by as much as 28%. As Z_Φ increases, results of the two categories gradually converge. Specifically, $Z_{\text{eff},m,tl}$ monotonically increases with Z_Φ.The reason is quite straightforward: Because $f_{i,\Phi}$ (Equation 18) remains constant throughout, increase in Z_Φ leads to increase in σ_Φ and $\sigma_{a,m}$ (Equation 17), hence increase in $Z_{\text{eff},m,tl}$. In contrast, $Z_{\text{eff},m,bq}$ exhibits a U-shaped pattern due to more intricate numerical changes: As Z_Φ increases, both $\lambda_{i,\Phi}$ (Equation 6) and $\sigma_{e,\Phi}$ increase, and the resulting $\sigma_{e,m}$ (Equation 11) does not change monotonically but instead has a minimum of 1.4315 barn at $Z_\Phi = 11$, hence the minimum value of $Z_{\text{eff},m,bq}$ at $Z_\Phi = 11$. This example demonstrates a potential usage scenario that favors the use of Taylor's formalism, in which materials with very similar elemental compositions need to be accurately differentiated.

3.2.2 | Phantom study

Figure 6 compared Z_{eff} maps of a physical phantom obtained under different formalisms. The phantom has a dimension of $30 \times 30 \times 20$ cm and includes a colon model with a total of 15 fold structures and 26 polyp structures. The phantom was scanned on SOMATOM Definition Flash (Siemens) using 80–140 kVp without filtration. The Z_{eff} map calculated by Van Abbema's formalism was expectedly in agreement with that by Bourque's. On both of these maps, Z_{eff} of the bone-equivalent material was the highest (13.2 ∼ 14.0), and that of the tissue-equivalent material (6.6 ∼ 7.0) was close to the air (7.7). Taylor's formalism generated a markedly different map: Although Z_{eff} of the air became slightly smaller (7.4) than Bourque's result, both tissue-equivalent (3.4 ∼ 3.6) and bone-equivalent materials (6.5 ∼ 6.7) had significantly lower values. This observation is in accord with our analysis in Section 2.1.5 that

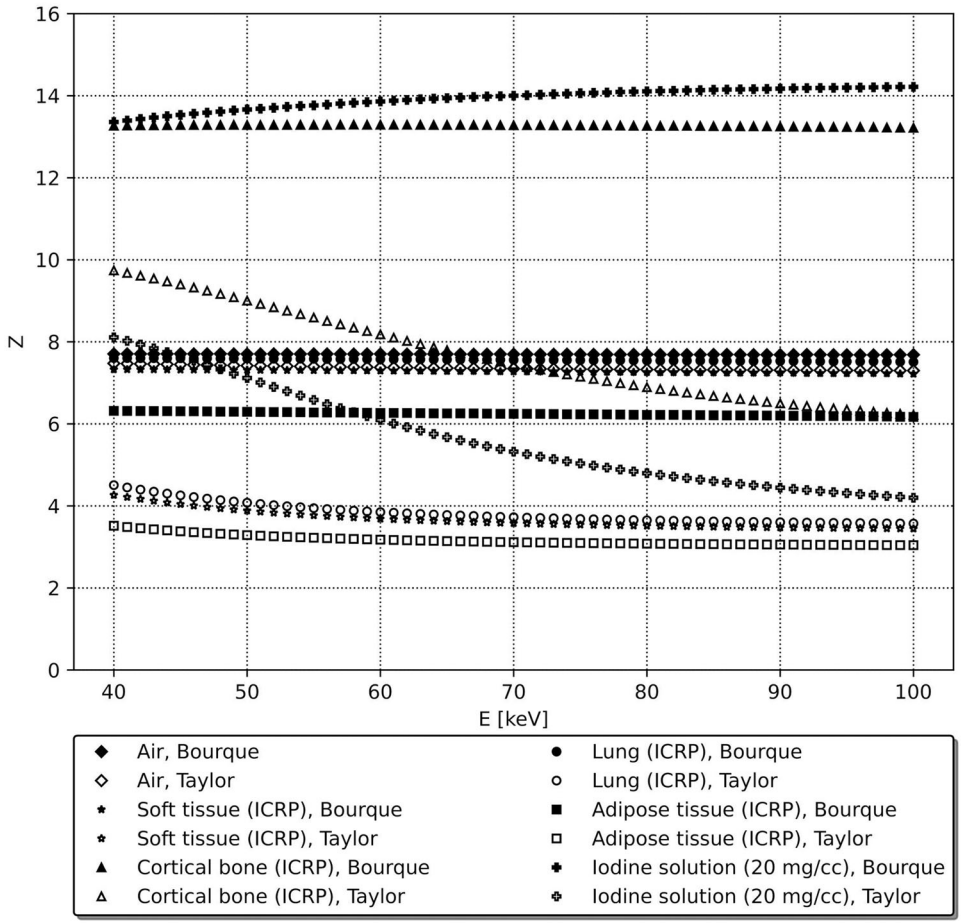

FIGURE 4 Z_{eff} values of several mixtures at photon energy 40 ~ 100 keV. Filled markers are data calculated by Bourque's formalism, and hollow markers by Taylor's. Markers of the same shape are data for the same material

materials containing hydrogen elements see greater discrepancy between Bourque's and Taylor's formalisms.

3.3 | Application of Z_{eff} calculation engine in 3DQI

3.3.1 | Kidney stone classification

One of the common applications of DECT is kidney stone classification, intended to differentiate uric acid (UA) stones from the calcium-containing non-UA stones.[26] UA stones ($C_5H_4N_4O_3$[27]) accounting for approximately 10% of the stone diseases are characterized by a smaller Z_{eff} and are usually treated medically.[26] Here we considered a patient with mixed type of kidney stones scanned on SOMATOM Definition Flash (Siemens) using 80–140 kVp with tin filtration.

The Z_{eff} map based on Bourque's formalism was calculated by our developed Z_{eff} engine using a pair of DECT images (Figure 7(a) and (b)). The Z_{eff} map was then superimposed on the CT image for the areas whose CT numbers exceed that of the soft tissue, shown in Figure 7(d). The Z_{eff} values of six common kidney stone materials, including pure UA, cystine, struvite, calcium oxalate dihydrate, calcium oxalate monohydrate, and hydroxyapatite were 6.92, 10.99, 12.43, 13.31, 13.77, and 16.05, respectively. A threshold of 7.3 was selected to differentiate UA (red) from non-UA (blue) components in the stone. The reference Z_{eff} image Figure 7(c) was derived from the commercial software Syngo.Via VB20A (Siemens) using the three-material decomposition method (urine, UA, and calcium). The resulting image overlaid with Bourque's Z_{eff} was in good agreement with the reference image.

The result by Van Abbema's formalism was consistent with Bourque's as expected. In comparison, the result by Taylor's formalism had limited accuracy: Although the bulk of the kidney stone was properly classified, some pixels within the kidney stone and within the bony structures were still not labeled correctly. The reason is that, for Taylor's formalism, the six common types of kidney stones were used as the application-specific base materials, among which cystine, struvite, calcium oxalate dihydrate, and calcium oxalate monohydrate have highly energy-dependent Z_{eff} values. The difference between

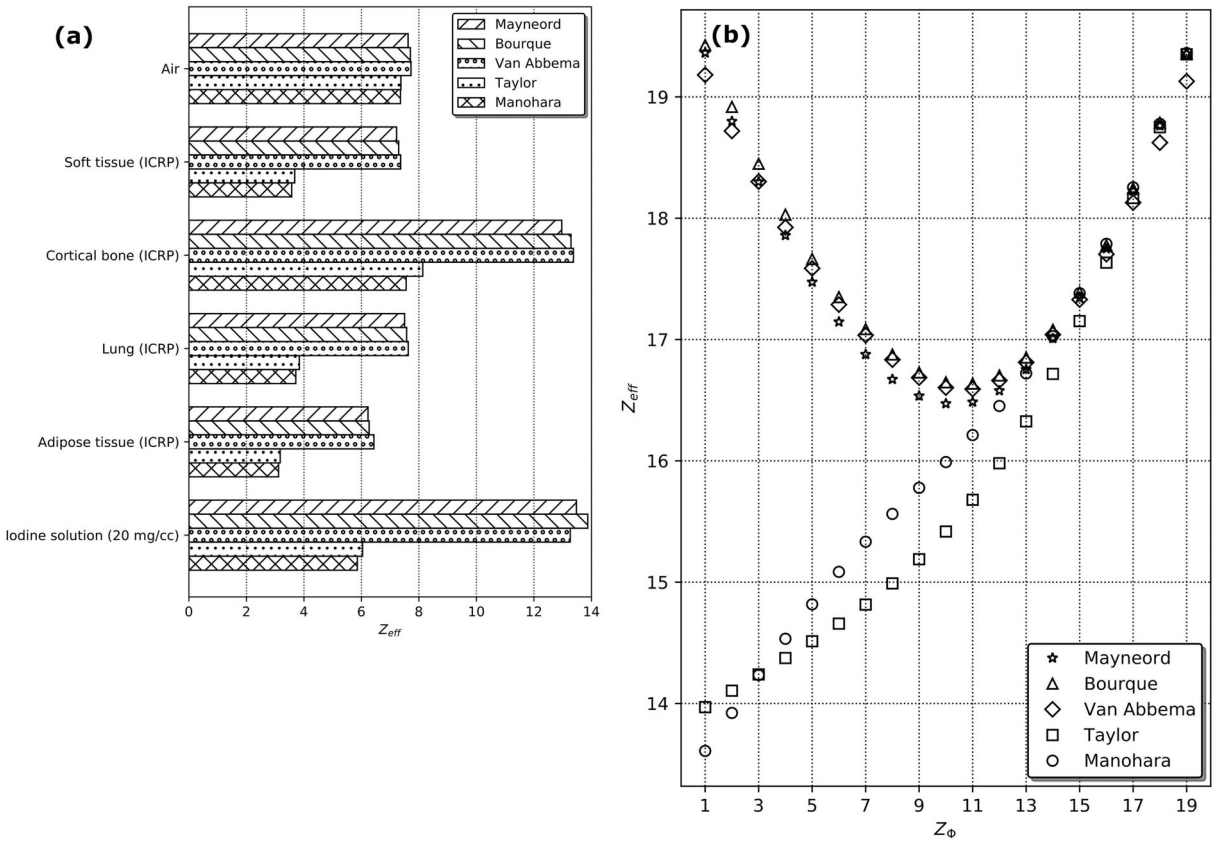

FIGURE 5 (a) Comparison of Z_{eff} values of several mixtures at photon energy 60.605 keV, calculated by different methods. (b) Z_{eff} values of a fictitious material $Ca\Phi_2$ as a function of Z_Φ (the atomic number of element Φ)

$Z_{\text{eff},m,tl}(E_{\text{high}})$ and $Z_{\text{eff},m,tl}(E_{\text{low}})$ can be as high as 18.8 ~ 29.4%. This went against the caveat in 2.2.4 and the result saw higher uncertainty.

3.3.2 | Colon electronic cleansing

In CT colonography (CTC), electronic cleansing (EC) is an advanced imaging processing technique to identify tagged fecal materials and subtract them from CTC images after image acquisition.[28] One of the major EC artifacts is the pseudo soft-tissue structures caused by under- or over-subtraction of air-tagging boundary, which is a mixture of air and tagged fecal residues caused by the partial volume effect. This air-tagging boundary not only has CT values significantly overlapping that of soft-tissue structures, but also may have gradient values that are close to those of soft-tissue structures,[29] which is the major cause of Type 2 artifacts in EC. The application of DECT has enabled the EC technique to differentiate tagged fecal materials and the air-tagging boundaries from colonic soft-tissue structures.[30]

This study applied the developed Z_{eff} engine to colon EC for a DECT scan, shown in Figure 8. The patient underwent a 24-hour bowel preparation with a low-fiber, low-residue diet, and oral administration of 150 ml of iodinated contrast agent. The DECT scan (SOMATON Definition Flash, Siemens) was performed using the low-dose imaging protocol: Tube A at 80 kVp/40 mAs and tube B at 140 kVp/15 mAs with tin filtration. The effective dose of this scan was estimated to be approximately 0.75 mSv. Using Taylor's formalism for Z_{eff} calculation, the Z_{eff} values of air ($Z_{\text{eff}} = 7.37$) and iodine tagging materials (such as 20 mg/ml: $Z_{\text{eff}} = 6.04$) were substantially higher than that of soft tissue ($Z_{\text{eff}} = 3.71$), as is shown in Figure 8(c). This allowed the tagged fecal materials to be accurately subtracted and soft-tissue structures such as the submerged polyp to be safely preserved.

4 | DISCUSSION

4.1 | Nonuniqueness of Z_{eff}

Z_{eff} is an artificial physical quantity used to extend Z from $\mathbb{N}$ to $\mathbb{R}$ for compounds and mixtures. Bonnin[8] recently proposed a generalized formulation of Z_{eff} that applies well to this study: For specific incident particles, energy ranges, and interactions, a material giving a monotonic signal $\Psi = \Psi(Z_{\text{eff}})$ is considered equivalent

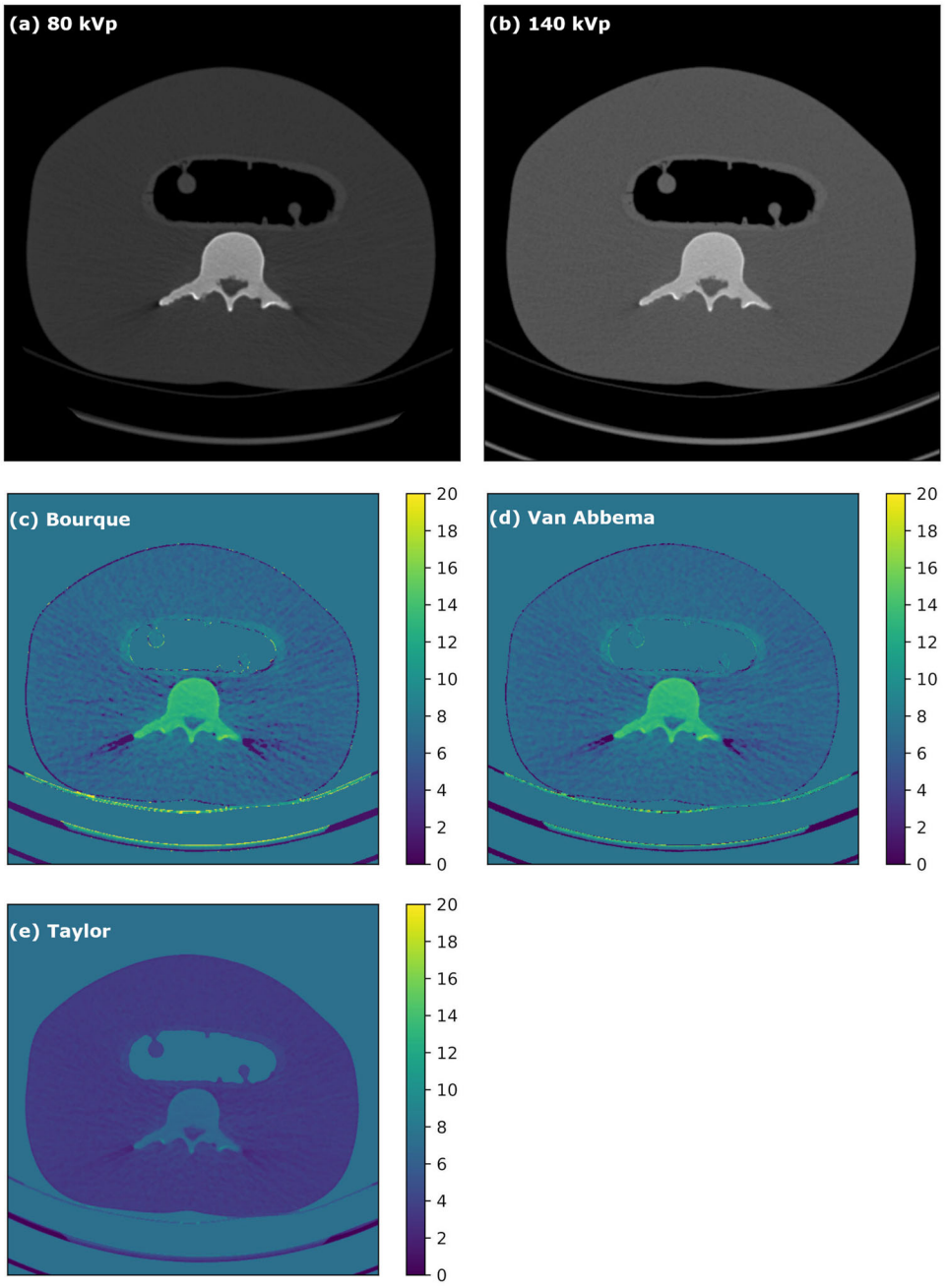

FIGURE 6 An abdomen phantom with a colon model. (a) and (b) A pair of DECT images, where (a) is the image of 80 kVp and (b) is the image of 140 kVp without filtration. (c) Z_{eff} map calculated using Bourque's formalism. (d) Using Van Abbema's formalism. (e) Using Taylor's formalism

to a fictitious element with $Z = Z_{\text{eff}}$ yielding the same signal. For the same material, different choices of the signal function give rise to different Z_{eff} values, and the choice has to be made with adequate justification according to the context of application.

Specifically, the DECT applications, such as (1) material differentiation with unknown elemental compositions, and (2) stopping power ratio estimate for proton therapy, need Z_{eff} to be as much energy-independent as possible. To that end, Bourque's formalism (based on the signal $\sigma_{e,m}$) and equivalently, Rutherford's and its derivatives, are the most appropriate options. For calculation of Z_{eff} of reference materials with known elemental compositions at the CT energy range, Mayneord's formalism is usually well suited due to its absolute independence from the signal $(\sigma_{PE} + \sigma_{INC})_m$ and the energy. In passing, Taylor (based on the signal $\sigma_{a,m}$) and Manohara's formalisms both feature intentional high energy dependence, but their study did not elucidate why this property is considered desirable in the first place and what applications may actually benefit from it.

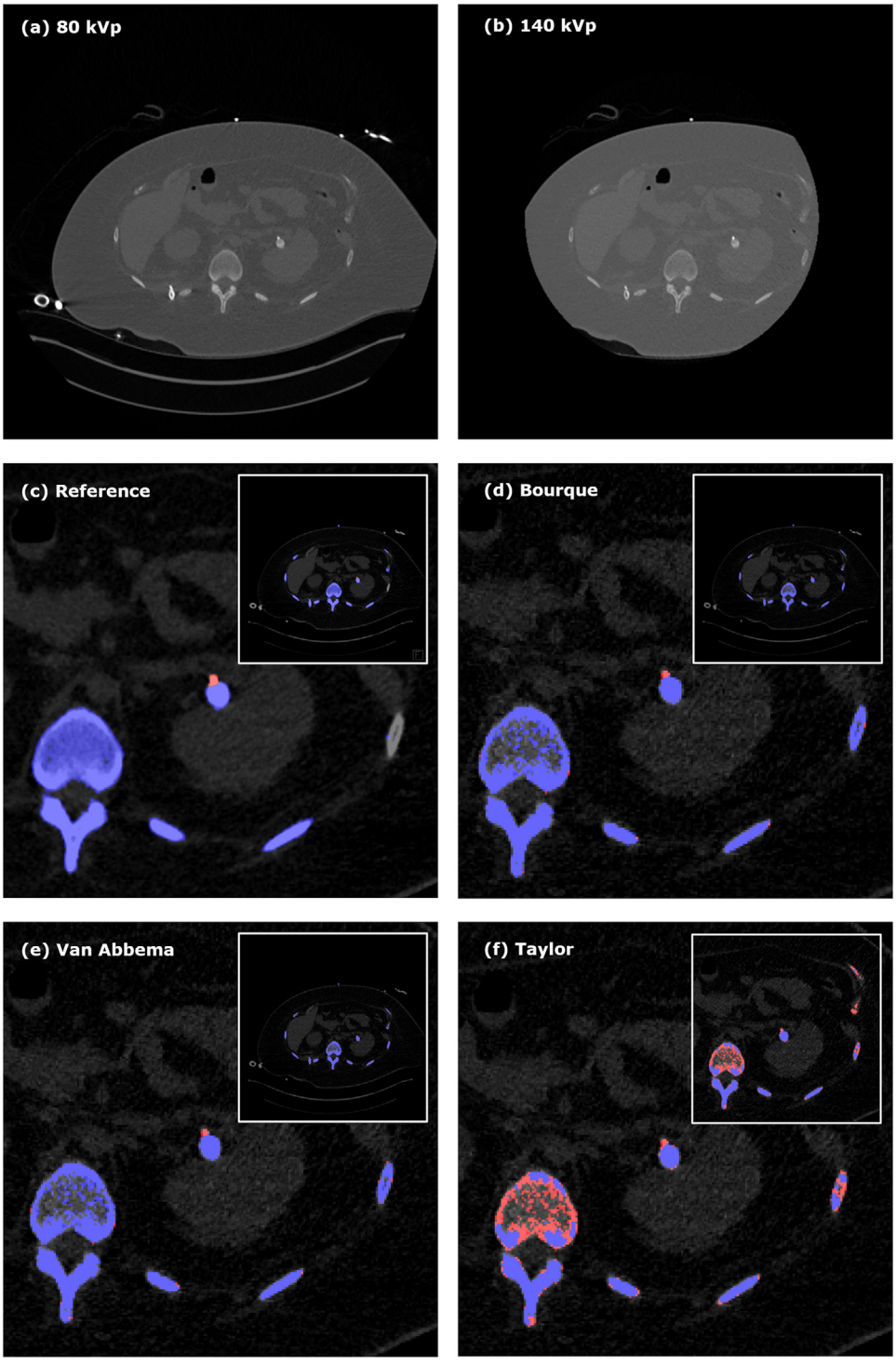

FIGURE 7 A 33 year-old patient with mixed type of kidney stones. (a) and (b) A pair of DECT images, where (a) is the image of 80 kVp and (b) is the image of 140 kVp with tin filtration. (c) Reference color-coded image calculated by the software Syngo.Via VB20A. Red is UA stone and blue is non-UA stone. (d) Image calculated by the Z_{eff} engine developed in this study, using Bourque's formalism. (e) Result of Van Abbema's formalism. (f) Result of Taylor's formalism

Besides the strict "equivalent signal"-based formalisms, Z_{eff} is also seen to be defined in somewhat loose forms, usually in Monte Carlo simulation where model coefficients of specific interactions need to be estimated for compounds and mixtures. For example, the general-purpose radiation transport code Geant4[31] has used the following two forms: (1) The trivial form given by Equation (24), used in the charged particle Urban multiple scattering model and Penelope photon pair production model; (2) $Z_{\mathrm{eff},m} = \sum_i w_i Z_i$, where w_i is the

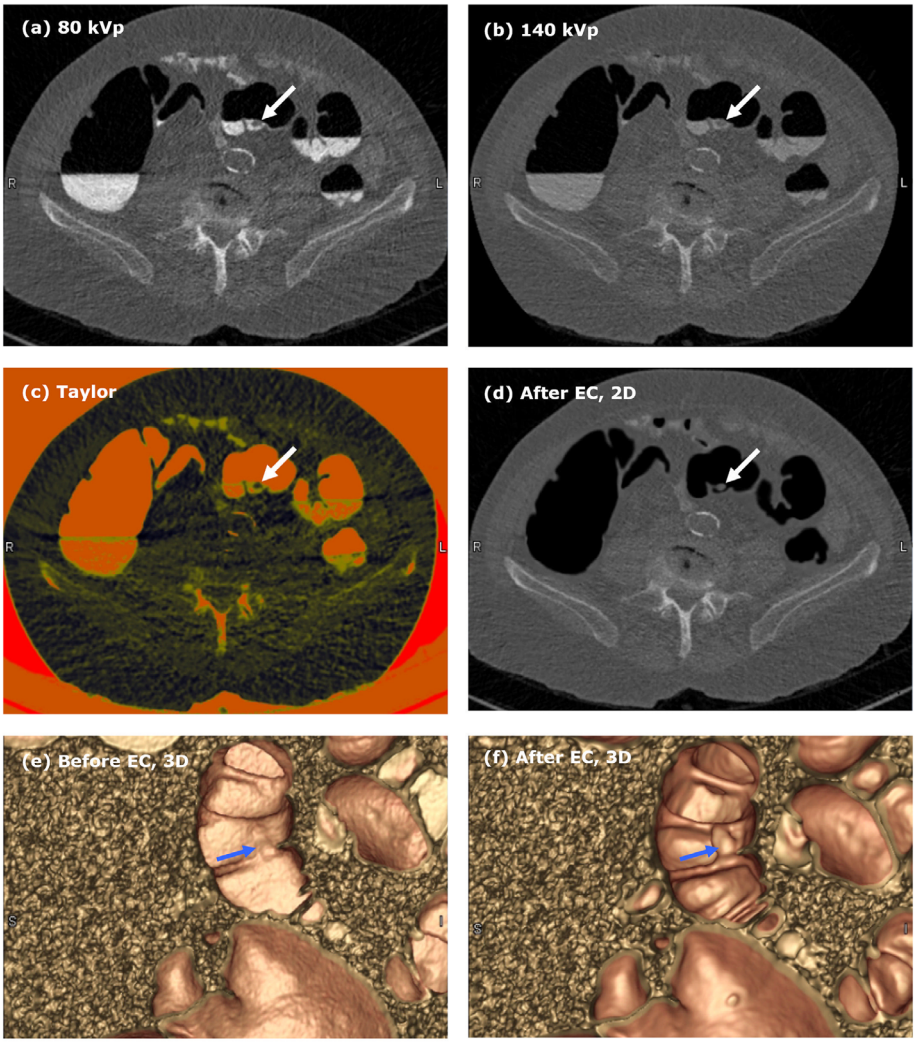

FIGURE 8 A 9-mm adenoma polyp confirmed by optical colonoscopy in a 59-year-old male patient. (a) and (b) A pair of DECT images, where (a) is the image of 80 kVp and (b) is the image of 140 kVp with tin filtration. The submerged polyp is pointed to by the white arrow. (c) Image calculated by the Z_{eff} engine developed in this study, using Taylor's formalism. (d) The fused image of (a) and (b) after Z_{eff}-based EC was applied. The submerged polyp pointed to by the white arrow was well preserved, and the air-tagging boundaries were clearly removed. (e) Image of 3D rendering of the colon before Z_{eff}-based EC was applied. (f) Image after Z_{eff}-based EC was applied. The submerged polyp pointed to by the blue arrow was clearly visualized

fraction of the *i*th element by weight, used in the charged particle energy loss fluctuation model. Another general-purpose radiation transport code EGSnrc[32] has chosen (3) $Z_{\text{eff},m} = \sqrt{\sum_i f_i Z_i (Z_i + 1)}$ in its bremsstrahlung model, where f_i is the fraction of the *i*th element by the number of atoms. An interesting research direction is to investigate whether different formalisms of Z_{eff} reviewed herein (microscopic cross-sections would be replaced by stopping power for charged particles) may improve these interaction models and to what extent.

4.2 | Limitations of the study

First, as a proof-of-principle demonstration of the table lookup method, we used manufacturer-provided mean energy values of the high and low kVp spectra, while in practice the spectrum information should be obtained experimentally. For Bourque's formalism, the stoichiometric calibration[12] involving the use of a calibration phantom should be conducted to determine $Z_{\text{eff}}(\Gamma)$ and avoid spectrum measurement for good.

Second, in our developed API, all Z_{eff} implementations except for Mayneord's formalism have varying degrees of energy dependence, making the results always associated with certain level of uncertainty. Detailed uncertainty analysis has not been added to our API yet. Bourque[12] conducted a systematic, theoretical uncertainty analysis for their formalism that will help with our implementation, while a similar analysis is still lacking for Taylor's formalism. As a rule of thumb, for Taylor's formalism the difference between Z_{eff} values at the mean

energy of the high and low kVp spectra is on the order of $6 \sim 12\%$ for practical CT applications, but may go beyond 25% for bones when the tin filtration is applied to the high kVp. For Bourque's formalism, the difference is remarkably smaller, generally between 0.3% and 0.8% for all common biological materials and all energy settings tested. Given that changing from σ_a to $\sigma_{e,m}$ leads to a significantly better Z_{eff} for DECT applications, it is tempting to push this further by parameterizing $\Psi(Z_{\text{eff}}) = \frac{\sum_i n_i \sigma_i}{\sum_i n_i Z_i^k}$, where $k > 0, k \in \mathbb{R}$. Seeking an optimal k that minimizes energy dependence of Z_{eff} is an interesting research topic.

5 | CONCLUSION

This paper renews the understanding of several highly cited formalisms of Z_{eff} and analyzes their connection and cause of discrepancy. The following conclusions can be drawn: (1) Previous study by Taylor[14] gave rise to a misconception that Mayneord's formalism is wrong. This is untrue. The power-law formula is in fact a favorably simple analytical expression with solid theoretical footing. (2) Bourque's formalism is based on parameterization of the average electron microscopic cross-section σ_e and uses the fraction of electron numbers λ as the weight function. The weak energy dependence of the calculated Z_{eff} naturally lends itself to material differentiation for DECT. Bourque's formalism, with the added advantage of being mathematically rigorous and physically meaningful, was found to be equivalent to the classic Mayneord's and Rutherford's formalisms. (3) Taylor's formalism uses the average atomic microscopic cross-section σ_a instead of σ_e and the fraction of atomic numbers f instead of λ to come up with Z_{eff} that is highly energy dependent. As a result, Taylor's formalism on paper is not a suitable candidate for DECT application. This study offers a practical workaround by using an RBF interpolation method. (4) The recent Manohara's formalism should be used with caution due to the problematic definition of effective electron microscopic cross-section.

This paper also introduces an efficient computation approach that pre-calculated Z_{eff} lookup tables to lift the burden of runtime calculation. This approach was adopted in the Z_{eff} engine developed for our 3DQI software. The Python API of our Z_{eff} calculation engine is open-source (https://github.com/3dqi/duo).

ACKNOWLEDGMENTS

This research was supported by National Cancer Institute (NCI) under award number R03CA223711.

CONFLICT OF INTEREST

The authors have no relevant conflicts of interest to disclose.

DATA AVAILABILITY STATEMENT

The data that support the findings of this study are available from the corresponding author on reasonable request.

REFERENCES

1. Mayneord W. The significance of the roentgen. *Acta Int Union Against Cancer*. 1937;2:271.
2. Spiers F. Effective atomic number and energy absorption in tissues. *Br J Radiol*. 1946;19(218):52-63.
3. Cunningham JR, Johns HE. *The Physics of Radiology*. Springfield: Charles C. Thomas; 1983.
4. Attix FH. *Introduction to Radiological Physics and Radiation Dosimetry*. Hoboken, NJ: John Wiley & Sons; 2008.
5. Saito M, Sagara S. A simple formulation for deriving effective atomic numbers via electron density calibration from dual-energy CT data in the human body. *Med Phys*. 2017;44(6):2293-2303.
6. McCollough CH, Boedeker K, Cody D, et al. Principles and applications of multi-energy CT report of AAPM Task Group 291. *Med Phys*. 2020;47:e881-e912.
7. Han D, Siebers JV, Williamson JF. A linear, separable two-parameter model for dual energy CT imaging of proton stopping power computation. *Med Phys*. 2016;43(1):600-612.
8. Bonnin A, Duvauchelle P, Kaftandjian V, Ponard P. Concept of effective atomic number and effective mass density in dual-energy X-ray computed tomography. *Nucl Instrum Methods Phys Res B*. 2014;318:223-231.
9. Rutherford R, Pullan B, Isherwood I. Measurement of effective atomic number and electron density using an EMI scanner. *Neuroradiology*. 1976;11(1):15-21.
10. Torikoshi M, Tsunoo T, Sasaki M, et al. Electron density measurement with dual-energy x-ray CT using synchrotron radiation. *Phys Med Biol*. 2003;48(5):673.
11. Bazalova M, Carrier J-F , Beaulieu L, Verhaegen F. Dual-energy ct-based material extraction for tissue segmentation in Monte Carlo dose calculations. *Phys Med Biol*. 2008;53(9):2439.
12. Bourque AE, Carrier J-F, Bouchard H. A stoichiometric calibration method for dual energy computed tomography. *Phys Med Biol*. 2014;59(8):2059.
13. Yang N, Leichner P, Hawkins W. Effective atomic numbers for low-energy total photon interactions in human tissues. *Med Phys*. 1987;14(5):759-766.
14. Taylor M, Smith R, Dossing F, Franich R. Robust calculation of effective atomic numbers: the auto-zeff software. *Med Phys*. 2012;39(4):1769-1778.
15. Manohara S, Hanagodimath S, Thind K, Gerward L. On the effective atomic number and electron density: a comprehensive set of formulas for all types of materials and energies above 1 keV. *Nucl Instrum Methods Phys Res Sect B*. 2008;266(18):3906-3912.
16. Hine GJ. Secondary electron emission and effective atomic numbers. *Nucleonics (US) Ceased Publ*. 1952;10:9–15.
17. Landry G, Seco J, Gaudreault M, Verhaegen F. Deriving effective atomic numbers from DECT based on a parameterization of the ratio of high and low linear attenuation coefficients. *Phys Med Biol*. 2013;58(19):6851-6866.
18. Landry G, Reniers B, Granton PV, et al. Extracting atomic numbers and electron densities from a dual source dual energy CT scanner: experiments and a simulation model. *Radiother Oncol*. 2011;100(3):375-379.
19. Van Abbema JK, Van der Schaaf A, Kristanto W, Groen JM, Greuter MJ. Feasibility and accuracy of tissue characterization with dual source computed tomography. *Phys Med*. 2012;28(1):25-32.
20. Jeffreys H, Jeffreys B. Weierstrass's theorem on approximation by polynomials" and "Extension of Weierstrass's approximation theory." *Methods of Mathematical Physics*. Cambridge University Press; 1988.

21. Rao BT, Raju M, Narasimham K, Parthasaradhi K, Rao BM. Interaction of low-energy photons with biological materials and the effective atomic number. *Med Phys*. 1985;12(6):745-748.
22. AMD. HIP Programming Guide, 2020.
23. Berger MJ, Coursey J, Zucker M, Chang J. *Stopping-Power and Range Tables for Electrons, Protons, and Helium Ions*. NIST Physics Laboratory Gaithersburg, MD; 1998.
24. Brown DA, Chadwick M, Capote R, et al. Endf/b-viii. 0: the 8th major release of the nuclear reaction data library with cielo-project cross sections, new standards and thermal scattering data. *Nucl Data Sheets*. 2018;148:1-142.
25. Manohara S, Hanagodimath S, Gerward L. The effective atomic numbers of some biomolecules calculated by two methods: a comparative study. *Med Phys*. 2009;36(1):137-141.
26. Hartman R, Kawashima A, Takahashi N, et al. Applications of dual-energy CT in urologic imaging: an update. *Radiologic Clinics*. 2012;50(2):191-205.
27. Qu M, Jaramillo-Alvarez G, Ramirez-Giraldo JC, et al. Urinary stone differentiation in patients with large body size using dual-energy dual-source computed tomography. *Eur Radiol*. 2013;23(5):1408-1414.
28. Zalis ME, Hahn PF. Digital subtraction bowel cleansing in CT colonography. *Am J Nucl Roentgenol*. 2001;176(3):646-648.
29. Cai W, Yoshida H, Zalis ME, Näppi, JJ, Harris GJ. Informatics in radiology: electronic cleansing for noncathartic CT colonography: a structure-analysis scheme. *Radiographics*. 2010;30(3):585-602.
30. Cai W, Lee, J-G, Zhang D, Kim SH, Zalis M, Yoshida H. Electronic cleansing in fecal-tagging dual-energy CT colonography based on material decomposition and virtual colon tagging. *IEEE Trans Biomed Eng*. 2014;62(2):754-765.
31. Agostinelli S, Allison J, Amako Ka, et al. GEANT4–a simulation toolkit. *Nucl Instrum Methods Phys Res Sect A*. 2003;506(3):250-303.
32. Rogers D, Kawrakow I, Seuntjens J, Walters B, Mainegra-Hing E. NRC user codes for EGSnrc. NRCC Report PIRS-702 (Rev. B); 2003.

How to cite this article: Liu T, Hong G, Cai W. A comparative study of effective atomic number calculations for dual-energy CT. *Med. Phys.*. 2021;1–16. https://doi.org/10.1002/mp.15166